# New evidences of in situ laser irradiation effects on $\gamma$-Fe2O3 nanoparticles: a Raman spectroscopic study

Yassine El Mendili, Jean-François Bardeau, Nirina Randrianantoandro, Alain Gourbil, Jean-Marc Greneche, A.-M. Mercier, Fabien Grasset

# New evidences of *in situ* laser irradiation effects on γ-$Fe_2O_3$ nanoparticles : a Raman spectroscopic study

**Y. El Mendili[1], J.-F. Bardeau[1*], N. Randrianantoandro[1], A. Gourbil[1], J.-M. Greneche[1], A.-M. Mercier[2], F. Grasset[3]**

[1]Laboratoire de Physique de l'Etat Condensé UMR CNRS 6087, Université du Maine Avenue Olivier Messiaen, 72085 Le Mans Cedex 9, France
[2]Laboratoire des Oxydes et Fluorures UMR CNRS 6010, Université du Maine, Avenue Olivier Messiaen, 72085 Le Mans Cedex 9, France
[3]Université de Rennes 1, Unité Sciences Chimiques de Rennes, UMR UR1-CNRS 6226, Bât 10A, Campus de Beaulieu, 35042 Rennes Cedex, France

* *Correspondence to: Jean-François Bardeau,* Laboratoire de Physique de l'Etat Condensé UMR CNRS 6087, Université du Maine Avenue Olivier Messiaen, 72085 Le Mans Cedex 9, France. *E-mail: Jean-Francois.Bardeau@univ-lemans.fr*.

## Abstract

The nature of the physical mechanisms responsible for the structural modification of the γ-$Fe_2O_3$ nanoparticles under laser irradiation has been investigated by Raman spectroscopy. *In situ* micro-Raman measurements were carried out on as-prepared γ-$Fe_2O_3$ nanoparticles of about 4nm in size as a function of laser power and on annealed γ-$Fe_2O_3$ particles. A baseline profile analysis has clearly evidenced that the phase transition from maghemite into hematite is caused by local heating due to laser irradiation with an increase of grain sizes from 4nm in nanoparticles up to more than 177nm beyond 900 °C in a polycrystalline state as observed by X-ray diffraction.

## Introduction

Maghemite ($\gamma$–$Fe_2O_3$ phase) nanoparticles have received considerable attention in recent years due in particular to their ferrimagnetic and oxygen stability properties and to their biocompatibility as a contrast enhancer for magnetic resonance imaging or drug delivery career.[1,2,3] Although considerable amount of work has been devoted to $\gamma$–$Fe_2O_3$ nanoparticles, the mechanism of laser-induced phase transition for nanoparticle sizes below 10 nm has not yet been investigated, to the best of our knowledge. However, some difficulties were reported in the literature for the preparation and the stabilization[4,5] or degradation[6] of metastable pure ($\gamma$–$Fe_2O_3$) crystallites during heating treatment. It has been concluded that the transformation of metastable $\gamma$-$Fe_2O_3$ phase into the more stable hematite phase ($\alpha$-$Fe_2O_3$) within the temperature range 300 to 600°C is highly depending on the crystallinity and the particle size, i.e. the preparation method conditions,..etc. [7,8]

The purposes of the present study are a) to investigate the physical mechanisms associated to the phase transition of $\gamma$ -$Fe_2O_3$ nanoparticles induced by laser irradiation and b) to correlate the local structure modifications quantitatively with the evolution of vibrational spectra using the sensibility of Raman spectroscopy and a baseline profile analysis approach.

## Experimental

$\gamma$-$Fe_2O_3$ nanoparticles were prepared according to Massart's method[9] with cationic precursors used in the form of metallic salts soluble in the water. The non aggregated ultrafine powders were further heated in air up to 500, 900, 1200 and 1400°C successively for 30 min and then cooled down to room temperature.

The X-ray diffraction (XRD) measurements were performed with a Siemens D500 X-ray powder diffractometer using Cu-K$\alpha_{1,2}$ radiations ($\lambda_1$ = 1.5406 Å, $\lambda_2$= 1.5444 Å). XRD data were collected with a step size of 0.02° 2$\theta$ over the angular range from 20-100° 2$\theta$.

Both the structural (lattice parameters) and microstructural (average grain size, <D>, and r.m.s. microstrain, $\sqrt{\langle \varepsilon^2 \rangle}$ of crystalline domains) parameters were determined using the MAUD program with the full pattern XRD Rietveld fitting procedure combined with a Fourier analysis to describe the broadening of peaks. [10]

The Raman spectra were recorded at room temperature in the back scattering configuration on a T64000 Jobin-Yvon (Horiba) spectrometer under a microscope with a 100x objective focusing the 514 nm line from an Argon–Krypton ion laser (coherent, Innova). The spot size of the laser was estimated to 0.8 μm. Measurements using different laser output powers between 1mW and 600mW (corresponding to a laser power of 0.08mW-50mW on the sample) were carried out consecutively without moving the sample. Single spectra were recorded twice with an integration time varying between 400s and 600s.

## Results and Discussion

### Structure and diameter of the particles

The XRD patterns of the as-prepared maghemite powders and powdered samples resulting from heat treatments at 500, 900, 1200 and 1400 °C are illustrated in Fig.1. The typical X-ray peaks (220, 331, 400, 422, 511, 440) observed in the diffractogram are characteristic of the maghemite spinel-related structure (isomorphous of magnetite

SG Fd3m) [11]. The lattice parameter (Table 1) for the as-prepared γ-$Fe_2O_3$ powders was calculated to be a=8.358±0.005 Å (8.347 Å for microcrystalline γ-$Fe_2O_3$) while the average particle diameter, <D>, was estimated to be 4±2 nm, in agreement with Transmission Electron Microscopy (not shown there). For the heated powdered samples, the set of peaks are attributed to the rhombohedral structure (SG R-3cH) of the hematite phase. No extra peaks are clearly detected, suggesting that no impurity occurs in powders annealed beyond 500°C. As shown in Table 1, the lattice parameters for the heated samples are in fairly good agreement with the literature values of α-$Fe_2O_3$ crystalline structure a=5.008 Å, and c=13.647 Å, respectively. [12] The calculated average grain size of the particles increases from 35(5)nm at 500°C up to 177(10)nm beyond 900°C while the average microstrain decreases. Indeed, microstrain effects induced by crystalline defects, local stresses or expansion of the lattice and local fluctuations of chemical composition were mainly reduced by the thermally activated grain growth.

**Raman spectra**

Fig. 2 illustrates the Raman spectra of both as-prepared γ –$Fe_2O_3$ nanoparticles and powdered samples heated in a furnace at different temperature (500°C, 900°C and 1400°C). In the as-prepared nanoparticles, only three broad peaks at 350 $cm^{-1}$ ($T_1$) 500$cm^{-1}$ (E) and 720 $cm^{-1}$ ($A_1$) and magnon mode in the neighbourhood of 1300$cm^{-1}$ are clearly evidenced. [12,13,14,15,16]. Such a Raman structure clearly obeys to the symmetry rules established in the inverse spinel structure with a tetragonal sublattice distortion and the lack of resolution of the spectrum suggests a rather poor degree of cristallinity of the small maghemite nanoparticles.

At 500°C, the three vibrational modes related to maghemite phase vanish while seven other well defined lines appear at 225, 250, 290, 300, 415, 500 and 615$cm^{-1}$. These new vibration modes, characteristic of iron oxide hematite α-$Fe_2O_3$ crystalline phase[17], are also observed on powdered samples heated in a furnace at 900°C and 1400°C. The bandwidth decrease of those peaks, as the temperature increases, was previously reported by Beattie *et al*. [18]. Such a feature was then directly attributed to structural modifications and to the increase in particle size. In addition, the intense band at 1320$cm^{-1}$ is assigned to a two-magnon scattering arising from antiferromagnetic structure of α-$Fe_2O_3$[19].

Fig. 3 compares the Raman spectra of the maghemite samples recorded at different laser output powers ranged from 1mW up to 600mW. The intensity of maghemite vibrational modes decreases and gradually vanishes whereas at 15mW low intensity bands (119, 160, 220, 238, 285, 315, 400, 432, 485, 598, 659 and 800$cm^{-1}$) attributed to the hematite phase become stronger as the laser power increases and shift to higher wavenumber values. Stability of the Raman spectra has been verified for spectra recorded at 5mW and 600mW (output laser power) after 20min of irradiation and no modification has been observed.

**Data analysis**

The γ to α phase transition can be studied with more attention using a baseline profile analysis approach based on the difference between the intensity of two reference-like lines Lmin and Lmax centred at 340$cm^{-1}$ and 850$cm^{-1}$, respectively. The evolution of the calculated ($I_{Lmin}$ - $I_{Lmax}$) intensity is plotted versus the nominal output laser power in Fig. 4.

These results unambiguously evidence several regimes: as is shown in the inset of Fig.4, the significant increase of the low laser intensity (from 1mW for nominal output laser power or 0.08mW on the sample) suggests that the nanoparticles are immediately subjected to structural modifications. At 25mW (Fig.4), the behaviour observed on the curve clearly establishes a structural transition attributed straightforwardly to the maghemite into hematite phase transition. From 25mW to 100mW (Fig. 3), one can clearly see that the wavenumber and the bandwidth (FWHM) of the Raman modes are dependent of the laser power. The softening and broadening, measured up to $7cm^{-1}$ and $9cm^{-1}$ respectively, can be mainly attributed to strain effects resulting of a local temperature rising. The high-wavenumber shift (up to 16 $cm^{-1}$ for the $E_g$ mode) of Raman vibrational modes observed between 100 and 200mW could therefore be provoked by a sudden increase of grain size and structural relaxation phenomena associated with a long range reorganization. The singularity observed in Fig. 4 at 100mW and the decrease of the calculated ($I_{Lmin}$ - $I_{Lmax}$) intensity are likely due to the same phenomena. This assumption is supported by the well-defined and strong Raman intensity bands observed from 300 to 600mW (output laser power) suggesting a progressive crystallization of particles and the increase of grain sizes in a polycrystalline state as previously reported in literature[13,20] for various iron-oxide materials after thermal treatment. Similar behaviour has been verified on powdered samples heated in a furnace and in particular between 500°C and 900°C curves in Fig.2 where high-wavenumber shift up to $6cm^{-1}$ was observed.

The evolution of the bandwidths of stronger $A_1$ and $2E_g$ vibrational modes of hematite phase as function of thermal treatment and under laser irradiation are compared in Fig. 5. With regard to the excellent agreement between the bandwiths curves, there is no doubt that the crystallisation of the hematite phase induced by laser irradiation is purely due to a thermal effect resulting from light absorption[9]. This result is not so surprising since in micro-Raman experiments, where the laser light is focused on the micrometer-size area, the laser energy density can be very high. In our case, where laser output power is about 600mW, the laser energy density can be estimated (in a volume close to $1\mu m^3$) to be approximately 50 GWatt /$cm^3$. A rise in temperature of several hundreds of degrees can be reached easily under a microscope and induce thus significant structural changes in materials. The identical values of the bandwidths in Fig. 5 allow immediately to address quantitatively for $\alpha$-$Fe_2O_3$ the correspondence between the output laser power and the temperature of thermal treatment. Consequently, this result also suggests that the local temperature of sample heated under laser excitation can be directly estimated from the bandwidths of Raman vibrational modes.

## Conclusions

In summary, it is demonstrated by micro-Raman and X-ray diffraction measurements that the structural modification observed for $\gamma$-$Fe_2O_3$ nanoparticles under laser irradiation is due to a thermal effect associated with an increase of the grain sizes. Our investigations also revealed that even at low laser power, the effects of structural modifications are irreversible on nanoparticles and can be immediately evidenced from the Raman spectra. Consequently, our results show that much more attention has to be considered when either nanostructured materials or nanocomposites are investigated by means of laser based spectroscopy. Indeed, it is relatively easy to unintentionally heat a sample when using a microscope in which the laser light is focused to a small focal volume with a resulting high power density. For $\alpha$-$Fe_2O_3$, we show that a few mW output laser can easily induce significant structural changes.

## Acknowledgments

This work was supported from the *Collectivités Locales, Le Mans Métropole – Département de la Sarthe*. The *Centre de Compétence C'Nano Nord-Ouest* is also gratefully acknowledged for financial support.

## References


(1) A. F. Thünemann, D. Schütt, L. Kaufner, U. Pison, H. Möhwald, *Langmuir* **2006**, *22*, 2351.
(2) S. Mornet, S. Vasseur, F. Grasset, E. Duguet, *Journal of Materials Chemistry* **2004**, *14*, 2161.
(3) M. H. Sousa, J. C. Rubim, P. G. Sobrinho, F. A. Tourinho, *Journal of Magnetism and Magnetic Materials* **2001**, *225*, 67.
(4) M. A. G. Soler, G. B. Alcantara, F. Q. Soares, W. R. Viali, P. C. Sartoratto, J. R. L. Fernandez, S. W. D. Silva, V. K. Garg, A. C. Oliveira, P. C. Morais, *Surface Science* **2007**, *601*, 3921.
(5) P. P. C. Sartoratto, K. L. Caiado, R. C. Pedroza, S. W. D. Silva, P. C. Morais, *Journal of Alloys and Copounds* **2007**, *434*, 650.
(6) K. S. K. Varadwaj, M. K. Panigrahi, J. Ghose, *Journal of Solid State Chemistry* **2004**, *177*.
(7) S. Chaianansutcharit, O. Mekasuwandumrong, P. Praserthdam, *Crystal Growth & Design* **2006**, *6*, 40.
(8) M. D. Alcala, C. Real, *Solid State Ionics* **2006**, *177*, 955.
(9) R. Massart, *IEEE Transactions on Magnetics* **1981**, *17*, 1247.
(10) L. Lutterotti, *MAUD program, CPD, Newsletter (IUCr).* **2000**, *24, http://www.ing.unitn.it/~luttero/maud*.
(11) F. Delmonte, M. P. Morales, D. Levy, A. Fernandez, M. Ocana, A. Roig, E. Molins, K. Ogrady, C. J. Serna, *Langmuir* **1997**, *13*, 3627.
(12) C. Y. Min, Y. D. Huang, L. Liu, *Materials Letters* **2007**, *61*, 4756.
(13) O. N. Shebanova, P. Lazor, *Journal of Raman Spectroscopy* **2003**, *34*, 845.
(14) D. L. A. Defaria, S. V. Silva, M. T. Deoliveira, *Journal of Raman Spectroscopy* **1997**, *28*, 873.
(15) Y. Zhou, Z. J. Zhang, Y. Yue, *Materials Letters* **2005**, *59*, 3375.
(16) G. A. Ferguson, M. Hass, *Physical Review A* **1958**, *112*, 1130.
(17) S. Onari, T. Arai, K. Kudo, *Physical Review B* **1977**, *16*, 1717.
(18) I. R. Beattie, T. R. Gilson, *Journal of the Chemical Society A-Inorganic Physical Theoretical* **1970**, 980.
(19) C. G. Shull, W. A. Strauser, E. O. Wollan, *Physical Review A* **1951**, *83*, 333.
(20) B. Gillot, H. Nouaim, F. Mathieu, A. Rousset, *Materials Chemistry and Physics* **1991**, *28*, 389.

Table 1 : Refined values of lattice parameters of γ-$Fe_2O_3$ powders as prepared and after annealed in a furnace at different temperature (500°C, 900°C, 1200°C and 1400°C) and corresponding agreement factors.

| | a (A) | c (A) | <D> (nm) | $\sqrt{\langle \varepsilon^2 \rangle}$. | $R_{exp}$ | $R_w$ | $\chi_i^2$ |
|---|---|---|---|---|---|---|---|
| 1400 °C | 5.038±0.005 | 13.757±0.001 | 177±10 | $2.95 \times 10^{-4}$ | 11.97 | 22.24 | 3.45 |
| 1200 °C | 5.039±0.005 | 13.757±0.001 | 177±10 | $3.38 \times 10^{-4}$ | 10.16 | 17.78 | 3.06 |
| 900 °C | 5.040±0.005 | 13.751±0.005 | 177±10 | $4.80 \times 10^{-4}$ | 8.8 | 16.45 | 3.49 |
| 500 °C | 5.034±0.005 | 13.765±0.005 | 35±5 | $2.21 \times 10^{-3}$ | 8.36 | 10.74 | 1.65 |
| RT | 8.366±0.010 | | 4±2 | $2.9 \times 10^{-4}$ | 8.05 | 10.75 | 1.77 |

## Figure captions:

Figure 1. XRD patterns of γ-$Fe_2O_3$ powders as prepared and heated in the temperature range of 500–1400◦C.

Figure 2. Raman spectra of as-prepared γ –$Fe_2O_3$ nanoparticles and powdered samples heated in a furnace at different temperature (500°C, 900°C and 1400°C). The Raman spectra were recorded at 0.4mW on the sample.

Figure 3. Evolution of Raman spectra of $Fe_2O_3$ powder as laser power increases. Reference-like lines (dashed lines) Lmin and Lmax are centered respectively at 340 $cm^{-1}$ and 850 $cm^{-1}$.

Figure 4. Evolution of the calculated ($I_{Lmin}$ - $I_{Lmax}$) intensity versus nominal output laser power.

Figure 5. Temperature (■) and laser power (▲) dependence of the bandwidths $A_1$ (~225 $cm^{-1}$) and $2E_g$ (~290 $cm^{-1}$) of hematite.

**Figure 1.**

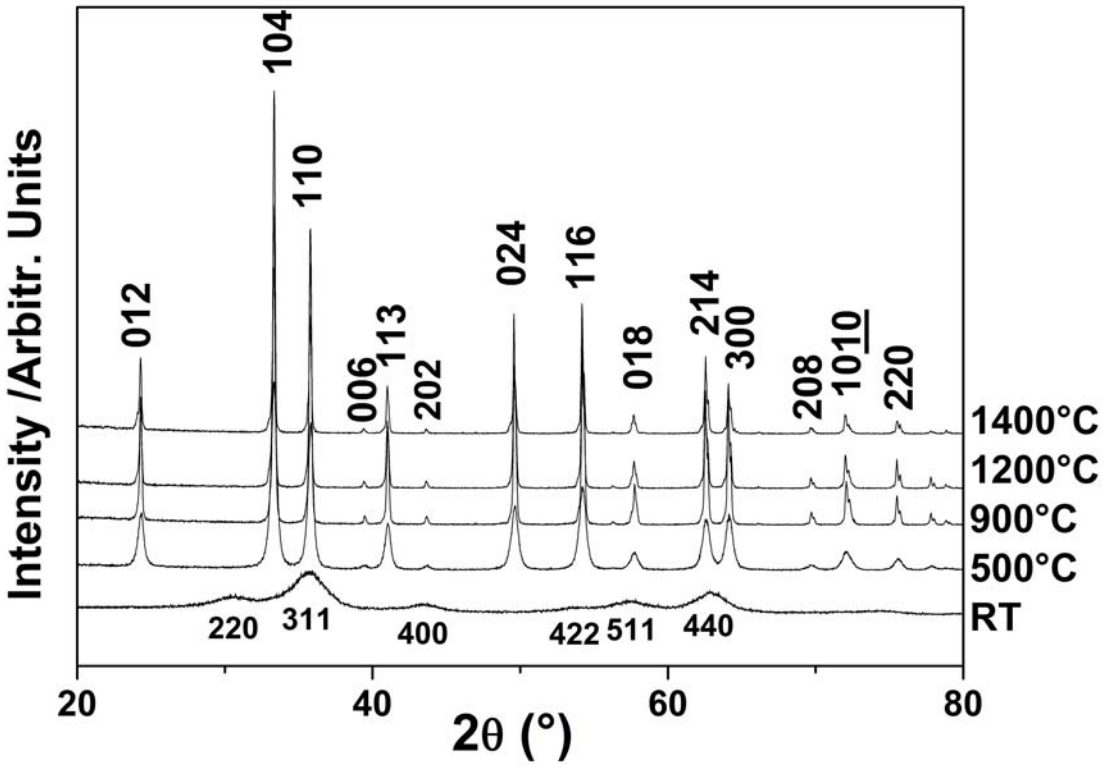
Intensity /Arbitr. Units
012
104
110
006
113
202
024
116
018
214
300
208
1010
220
220
311
400
422
511
440
1400°C
1200°C
900°C
500°C
RT
20
40
60
80
2θ (°)

**Figure 2.**

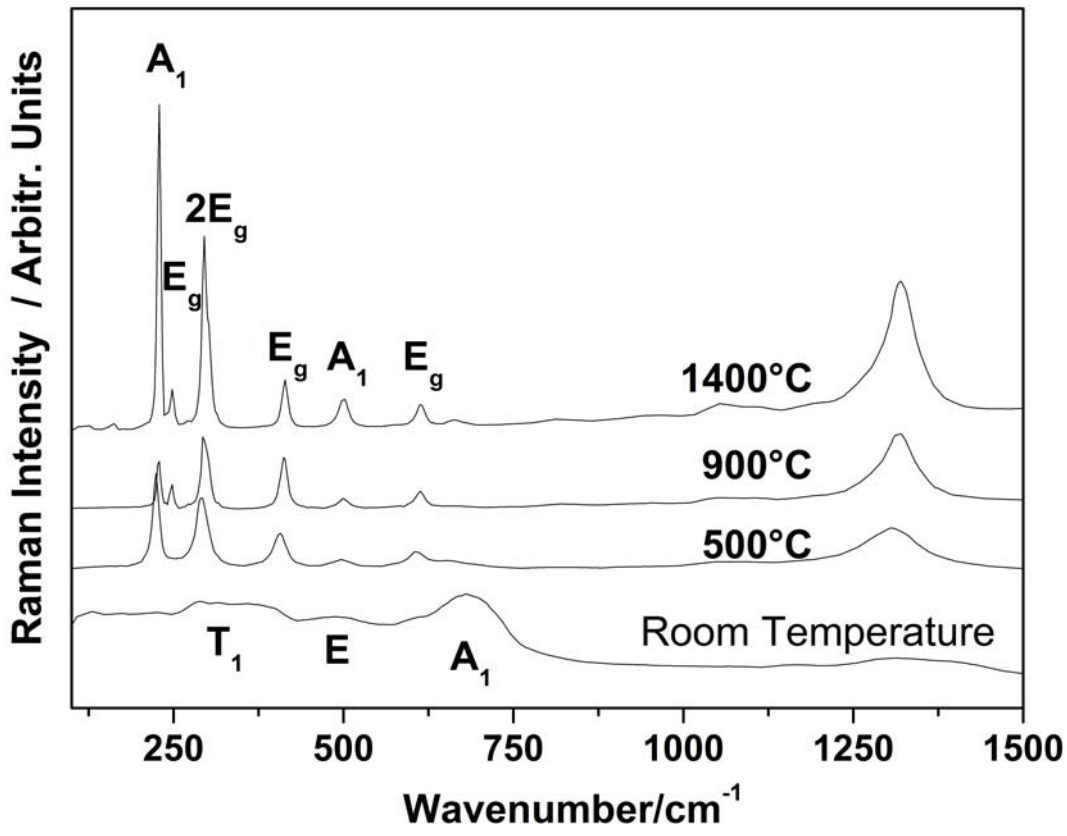
Raman Intensity / Arbitr. Units
A1
2Eg
Eg
Eg
A1
Eg
1400°C
900°C
500°C
Room Temperature
T1
E
A1
250
500
750
1000
1250
1500
Wavenumber/cm-1

**Figure 3.**

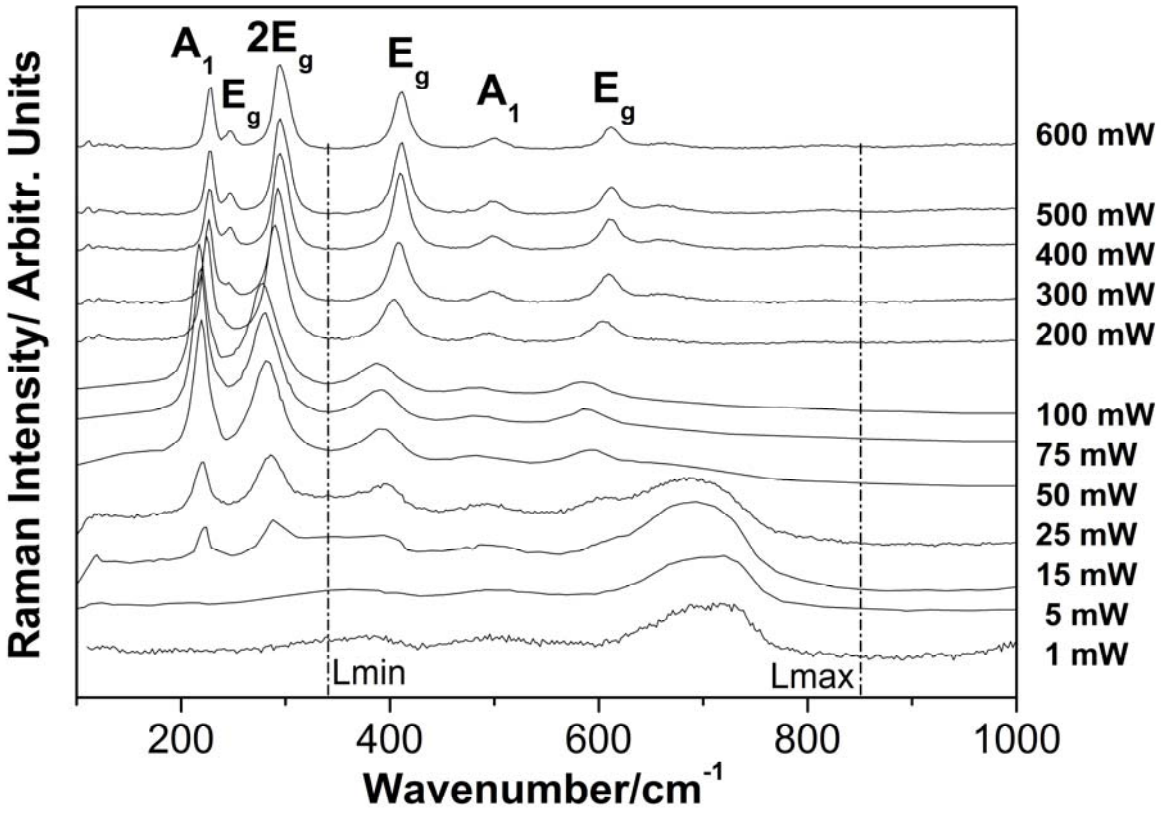
A1
Eg
2Eg
Eg
A1
Eg
600 mW
500 mW
400 mW
300 mW
200 mW
100 mW
75 mW
50 mW
25 mW
15 mW
5 mW
1 mW
Lmin
Lmax
Raman Intensity/ Arbitr. Units
200
400
600
800
1000
Wavenumber/cm-1

**Figure 4.**

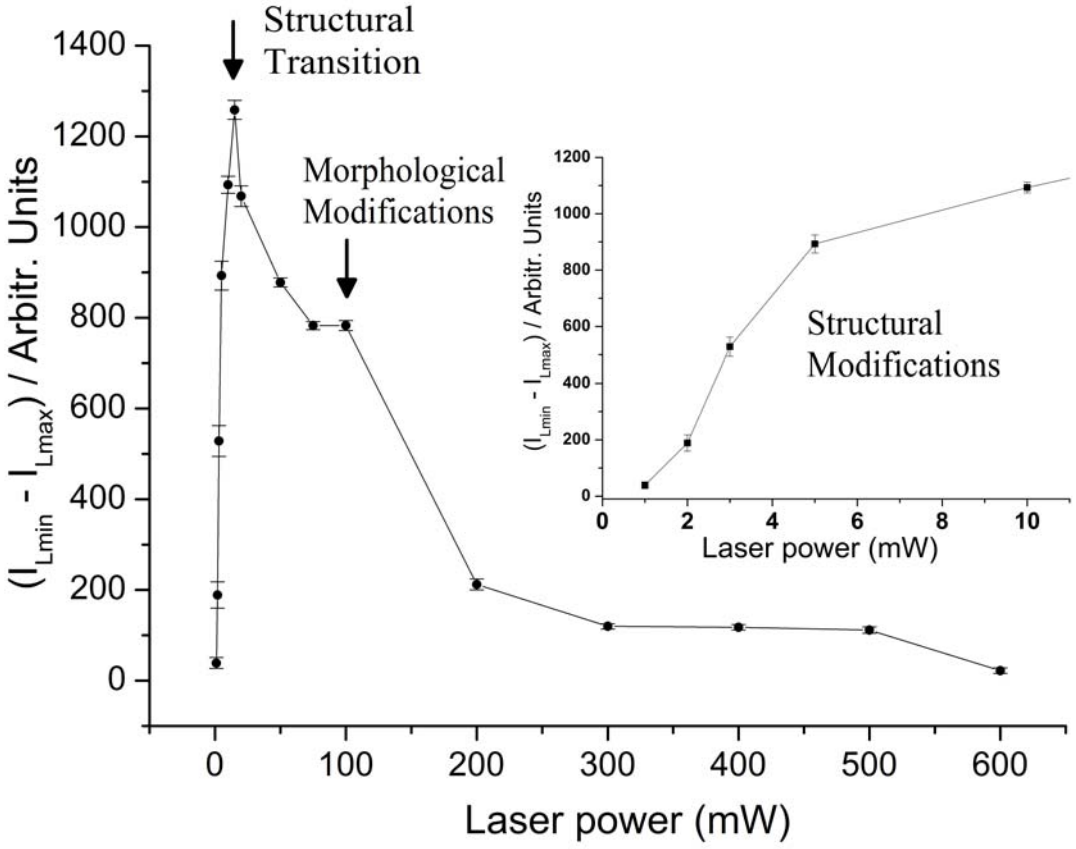
Structural
Transition
Morphological
Modifications
Structural
Modifications
(I_Lmin - I_Lmax) / Arbitr. Units
Laser power (mW)
0
200
400
600
800
1000
1200
1400
0
100
200
300
400
500
600
0
2
4
6
8
10

**Figure 5.**

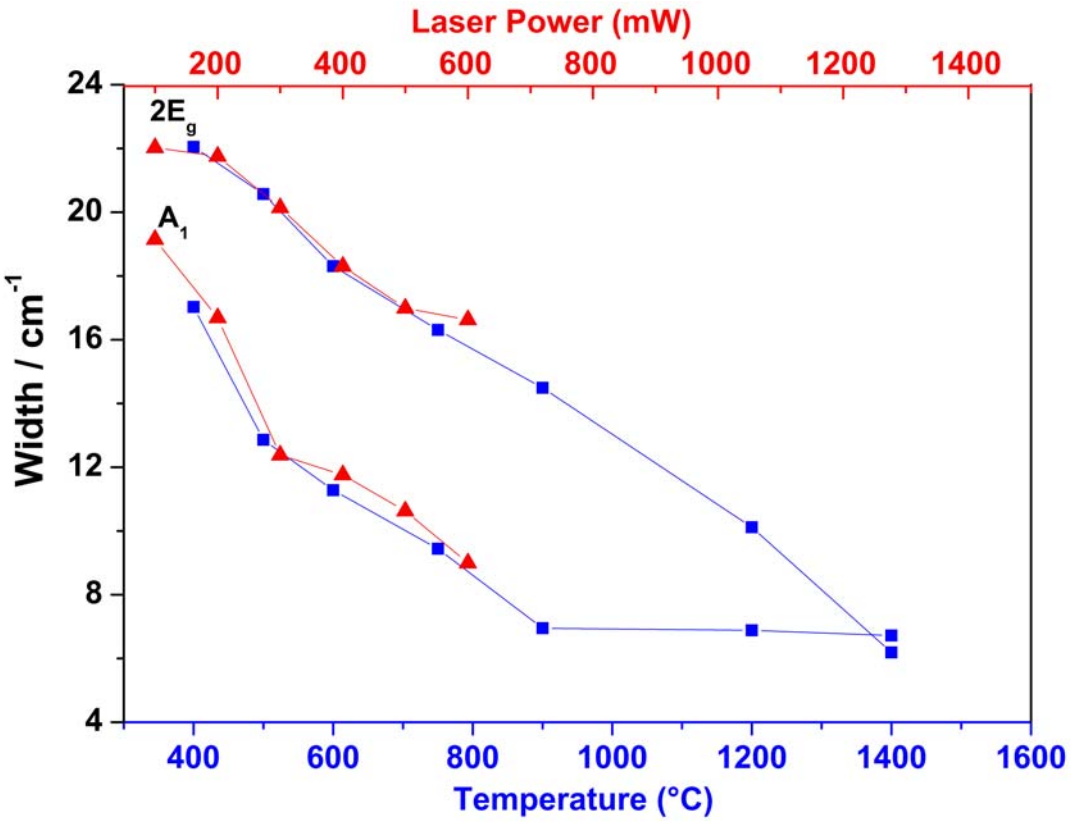
Laser Power (mW)
200
400
600
800
1000
1200
1400
24
20
16
12
8
4
2E$_g$
A$_1$
Width / cm$^{-1}$
400
600
800
1000
1200
1400
1600
Temperature (°C)